Optimization of a Spherical Mechanism for a Minimally Invasive Surgical Robot: Theoretical and Experimental Approaches

Mitchell J. H. Lum, Jacob Rosen* , Mika N. Sinanan, and
Blake Hannaford

Abstract—With a focus on design methodology for developing a compact and lightweight minimally invasive surgery (MIS) robot manipulator, the goal of this study is progress toward a next-generation surgical robot system that will help surgeons deliver healthcare more effectively. Based on an extensive database of *in-vivo* surgical measurements, the workspace requirements were clearly defined. The pivot point constraint in MIS makes the spherical manipulator a natural candidate. An experimental evaluation process helped to more clearly understand the application and limitations of the spherical mechanism as an MIS robot manipulator. The best configuration consists of two serial manipulators in order to avoid collision problems. A complete kinematic analysis and optimization incorporating the requirements for MIS was performed to find the optimal link lengths of the manipulator. The results show that for the serial spherical 2-link manipulator used to guide the surgical tool, the optimal link lengths (angles) are (60°, 50°). A prototype 6-DOF surgical robot has been developed and will be the subject of further study.

Index Terms—Isotropy, Jacobian, minimally invasive surgery, optimization, serial mechanism, spherical mechanism, surgical robot.
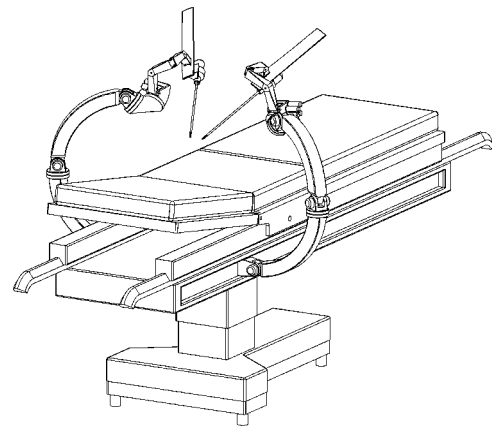
Fig. 1.   The complete manipulator system will consist of a micro-macro configuration. The "C-arm" macro-manipulator will position the dexterous micro-manipulator optimized in this paper.

I. INTRODUCTION

For decades, surgery and robotics progressed along parallel paths. Minimally invasive surgery (MIS) techniques revolutionized the way a significant number of surgical interventions are being performed. Progress in teleoperation has integrated the human into robotic systems. Only in the last decade have surgery and robotics reached respective levels of maturity to allow safe assimilation between them. As a result of extensive research in academia [1]–[12] and industry, robotic surgery can now be performed in the clinical setting. This will lead to a new kind of operating room with the potential for surgical innovation long into the future [13]. Two commercial systems for minimally invasive abdominal and thoracic surgery, da Vinci by Intuitive Surgical [14]–[16] and ZEUS by Computer Motion [17], [18] have been used in human surgery throughout the United States and Europe.

Intuitive Surgical's da Vinci as well as other robotic systems (e.g., [19]) implemented a remote center parallel mechanism, whereas Computer Motion's Zeus uses a serial chain in a SCARA-like configuration. One shortcoming of the existing systems is that they are large and cumbersome, occupying large volumes around the OR table and above the patient. These systems are subject to robot-robot collisions. The user interface may be enhanced by the use of force-feedback control, however the large mass, inertia and drive friction of current systems makes this addition difficult. Farz *et al.* [10] and Li *et al.* [11] have developed a 3-DOF parallel mechanism for positioning an endoscopic

camera, but due to the kinematic configuration and joint design constraints, this mechanism does not provide a suitable range of motion to guide a surgical tool. Shi *et al.* [12] proposes a similar mechanism to ours, however, the nature of neither their optimization nor their performance criteria were discussed. In this paper we use an optimized spherical mechanism subject to requirements based on *in-vivo* surgical measurements for a new surgical robot.

Kurtz and Hayward [20] and Merlet [21] have performed extensive research in parallel mechanism analysis and optimization. Ouerfelli and Kumar [22] analyzed a parallel spherical mechanism that is most similar to the mechanism in this study. They optimized for the largest possible workspace, showing link lengths of $\pi/2$ to be ideal. The authors assumed link lengths of $\pi/2$ for four of the five links of the parallel spherical mechanism, and optimized on a single link. For this reason, their derivation and equations did not take into account all of the design parameters studied in this paper.

The manipulator optimized in this study is part of a larger system that utilizes a micro-macro approach. The serial manipulator was optimized in earlier work [23] but the current optimization was refined, so the results deviate from the previous study. The complete system consists of a "C-arm" macro positioner and a high dexterity micromanipulator as illustrated in Fig. 1. The micromanipulator is cable-actuated with dc brushless motors located on a stationary base in order to minimize the mass and inertia of the moving parts. The structures of both parallel and serial spherical mechanisms are evaluated for the required workspace of MIS procedures. The definition of the workspace was based upon extensive *in-vivo* measurements of force/torque and position/orientation of surgical tools obtained during MIS on porcine models [24]–[26].

II. METHODS

A. Experimental Evaluation

Adjustable aluminum mock-ups were fabricated to physically model the kinematics of the mechanisms being studied. The mock-ups were designed with adjustable link angles and an inner radius of 10 cm with the ability to be configured as parallel or serial manipulators (Fig. 2). A special sleeve located at the "end-effector" of the mechanism allows MIS tools to be inserted through the joint in a way that mimics the tools of a surgical robot. This setup allows the surgeon to utilize the tools in the same manner as in MIS while passively moving the mechanisms and assessing range of motion, self-collisions, robot-robot collisions and robot-patient collisions. Self-collision was of primary concern with
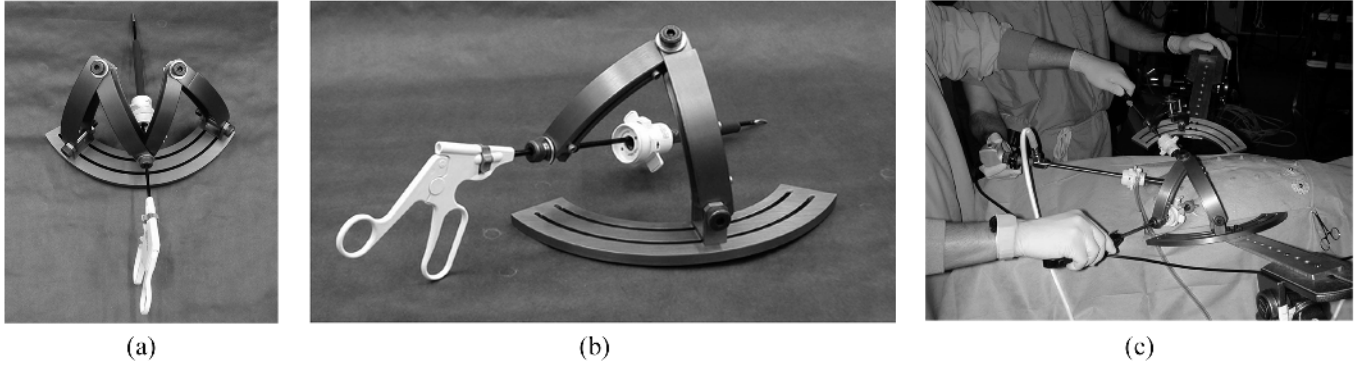
Fig. 2. Aluminum mock-up with adjustable link length and base length. The endoscopic tool is inserted into a guide located at mechanism apex in a configuration that allowed testing different design candidates in a real minimally invasive surgical setup. (a) Parallel configuration, (b) serial configuration, and (c) two serial configurations tested in a MIS setup. Although the robot manipulator will be teleoperated, in this evaluation the surgeon guides these passive mock-ups in order to evaluate the range of motion.

the parallel mechanisms; the two elbows (joints 3 and 4) were subject to collision thereby limiting the workspace. Robot-robot collisions were of concern because while each mechanism would be optimized separately, two or more manipulators will be present in the surgical scene. Robot-patient collisions are unacceptable for obvious safety reasons.

Using these mock-ups, different mechanism configurations were evaluated with link angles ranging from $60°$–$90°$ in $15°$ increments, in combinations of parallel and serial designs. (Note: Angles are described in degrees for a more intuitive representation, but all calculations were performed in radians). The first evaluations were performed on a training torso (Simulab, Seattle, WA) whereby the design candidate was moved through its entire range of motion. Collision problems for each candidate were assessed. Based on these initial results, surgeons selected the best candidates and *in-vivo* suturing and tissue manipulation tasks were performed on an animal through the mechanism [Fig. 2(c)]. This experimental protocol was performed to verify that the mechanism would have sufficient range of motion without collision problems.

B. Manipulator Kinematics

1) Spherical Mechanism—Conventions and Notations: Since the experimental evaluation showed that two parallel mechanisms could potentially collide in a MIS setup, we proceeded with only the derivation and optimization of a serial arm configuration. For the complete kinematic analysis of the parallel mechanism, see [27].

In the class of spherical mechanisms, all links' rotation axes intersect at either a single point or at infinity, referred to as the mechanism's remote center of rotation. Following the numbering scheme established in [22], we consider the serial mechanism to be one side of the parallel mechanism with two actuated joints numbered 1 and 3, and the end-effector at joint 5. Fig. 3 shows the assignment of frames, joints and links of the serial manipulator. Kinematic analysis of this configuration is independent of the sphere's radius, however, from a practical perspective the radius of the sphere should be kept as small as possible to minimize the overall size of the mechanism and adverse dynamic effects. As configured for MIS, the end-effector (surgical tool) is inserted through joint 5. The two joint angles, θ_1 and θ_3, determine the orientation of the end-effector in space. The center of the sphere serves as the origin for all reference frames of the mechanism's links. Thus, the transformations between the mechanism links' coordinate frames can be expressed as pure rotations. Frames are assigned to the mechanism joints based on the Denavit-Hartenberg (D-H) frames convention (Table I) such that the z-axis of the nth frame points outward along the nth joint [28]. When $\theta_1 = 0$ Link_{13} lies in a plane perpendicular to the
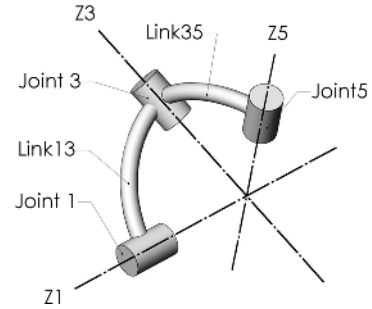

Fig. 3. Spherical mechanism: link and joint coordinate frame assignment, serial manipulator. When $\theta_1 = 0$ and $\theta_3 = 0$, the first link lays in plane perpendicular to the plane created by z_0 and x_0, and the second link is folded back on the first.

TABLE I
SERIAL MANIPULATOR D-H PARAMETERS—SEE FIG. 3 FOR ILLUSTRATION

$i-1$	i	$i+1$	α_{i-1}	θ_i
$0'$	1	3	0	θ_1
1	3	5	$-\alpha_{13}$	θ_3
3	5	—	α_{35}	$\theta_5 = 0$

plane created by intersecting axes z_0 and x_0. When $\theta_3 = 0$, Link_{35} is folded back onto Link_{13}

2) Forward Kinematics: Given the two joint angles θ_1 and θ_3, the forward kinematics of the 2R serial mechanism define the orientation of the end-effector frame. Rather than expressing the entire orientation of the end-effector frame, it is sensible to express a vector that is collinear to the end-effector (surgical tool) axis, z_5. This vector is expressed in Frame 5 as $^5 u_z = [0\ 0\ 1]^T$. The vector $^{0'} u$ has its origin at the center of the sphere, and points along the mechanism's end-effector, representing the orientation of the surgical tool expressed in the base frame.

$$^{0'}u = \begin{bmatrix} ^{0'}u_x \\ ^{0'}u_y \\ ^{0'}u_z \end{bmatrix} = {}^{0'}_5 R \begin{bmatrix} 0 \\ 0 \\ 1 \end{bmatrix}$$

$$= \begin{bmatrix} c\theta_1 s\theta_3 s\alpha_{35} + s\theta_1 c\theta_3 c\alpha_{13} s\alpha_{35} - s\theta_1 s\alpha_{13} c\alpha_{35} \\ s\theta_1 s\theta_3 s\alpha_{35} - c\theta_1 c\theta_3 c\alpha_{13} s\alpha_{35} + c\theta_1 s\alpha_{13} c\alpha_{35} \\ c\theta_3 s\alpha_{13} s\alpha_{35} + c\alpha_{13} c\alpha_{35} \end{bmatrix}. \quad (1)$$

3) Inverse Kinematics: Given the mechanism parameters (α_{i-1}) and the end-effector orientation expressed in Frame $0'$ $(^{0'}u)$ the inverse

kinematic equations solve for the mechanism joint angles (θ_i). Two solutions are available for any reachable $^{0'}u$ in the workspace. Using the Z component $^{0'}u_z$ [the third element of $^{0'}u$ (1)] results in

$$c\theta_3 = \frac{^{0'}u_z - c\alpha_{13}c\alpha_{35}}{s\alpha_{13}s\alpha_{35}}. \tag{2}$$

The two solutions for θ_3 are as follows:

$$\theta_{3a}, \theta_{3b} = atan2(\pm\sqrt{1 - c^2\theta3}, c\theta_3). \tag{3}$$

Using the expression for $^{0'}u_x$, $^{0'}u_y$ [the first and second element of $^{0'}u$ (1)] and the previous result, then solving for $sin\theta_1$ and $cos\theta_1$, results in

$$c\theta_1 = \frac{^{0'}u_x s\theta_3 s\alpha_{35} - {^{0'}u_y}(c\theta_3 c\alpha_{13} c\alpha_{35} - s\alpha_{13} c\alpha_{35})}{(s\theta_3 s\alpha_{35})^2 + (c\theta_3 c\alpha_{13} c\alpha_{35} - s\alpha_{13} c\alpha_{35})^2}$$
$$s\theta_1 = \frac{^{0'}u_y s\theta_3 s\alpha_{35} + {^{0'}u_x}(c\theta_3 c\alpha_{13} c\alpha_{35} - s\alpha_{13} c\alpha_{35})}{(s\theta_3 s\alpha_{35})^2 + (c\theta_3 c\alpha_{13} c\alpha_{35} - s\alpha_{13} c\alpha_{35})^2}$$
$$\theta_1 = atan2(s\theta_1, c\theta_1). \tag{4}$$

4) Jacobian Matrix: The Jacobian matrix $^A J$ mapping between joint velocities $(\dot{\theta}_i)$ and end-effector angular velocities $(^j\omega_5)$ can be expressed with respect to any frame (A) associated with the mechanism. The recursive formulation to derive the Jacobian matrix is expressed as follows [28]:

$$^5\omega_5 = {^5_1R}\begin{bmatrix} 0 \\ 0 \\ 1 \end{bmatrix}\dot{\theta}_1 + {^5_3R}\begin{bmatrix} 0 \\ 0 \\ 1 \end{bmatrix}\dot{\theta}_3 + \begin{bmatrix} 0 \\ 0 \\ 1 \end{bmatrix}\dot{\theta}_5. \tag{5}$$

Equation (5) is simplified into (6) defining the Jacobian matrix

$$\begin{bmatrix} ^5\omega_{5x} \\ ^5\omega_{5y} \\ ^5\omega_{5z} \end{bmatrix} = {^5 J_{\text{serial}}}\begin{bmatrix} \dot{\theta}_1 \\ \dot{\theta}_3 \\ \dot{\theta}_5 \end{bmatrix}$$
$$= \begin{bmatrix} j_{11} & j_{12} & 0 \\ j_{21} & j_{22} & 0 \\ j_{31} & j_{32} & 1 \end{bmatrix}\begin{bmatrix} \dot{\theta}_1 \\ \dot{\theta}_3 \\ \dot{\theta}_5 \end{bmatrix}$$
$$= \begin{bmatrix} ^5_1R\begin{bmatrix} 0 \\ 0 \\ 1 \end{bmatrix} & ^5_3R\begin{bmatrix} 0 \\ 0 \\ 1 \end{bmatrix} & \begin{bmatrix} 0 \\ 0 \\ 1 \end{bmatrix} \end{bmatrix}\begin{bmatrix} \dot{\theta}_1 \\ \dot{\theta}_3 \\ \dot{\theta}_5 \end{bmatrix}. \tag{6}$$

Our optimization is for a 2-DOF manipulator to orient the surgical tool. The advantage of expressing the Jacobian matrix in the end-effector frame (Frame 5) is that the last column of the matrix is $[0\ 0\ 1]^T$ for all poses and joint velocities. The 3-DOF Jacobian is then reduced to the 2-DOF Jacobian of interest by using only the upper 2×2 sub-matrix that relates the controlled joints (θ_1, θ_3) to the end-effector angular velocities (ω_x, ω_y)

$$\begin{bmatrix} ^5\omega_{5x} \\ ^5\omega_{5y} \end{bmatrix} = \begin{bmatrix} j_{11} & j_{12} \\ j_{21} & j_{22} \end{bmatrix}\begin{bmatrix} \dot{\theta}_1 \\ \dot{\theta}_3 \end{bmatrix}$$
$$j_{11} = -s\theta_3 s\alpha_{13}$$
$$j_{12} = 0$$
$$j_{21} = -c\theta_3 s\alpha_{13}c\alpha_{35} + c\alpha_{13}s\alpha_{35}$$
$$j_{22} = s\alpha_{35}. \tag{7}$$

Fig. 4. Workspace in MIS: an elliptical cone with vertex angles of 60° and 90° represents the workspace such that the endoscopic tool can reach any organ in the abdomen. The ports are placed such that the end-effector of the tools can access the target anatomy. In this illustration, the port is located at the center of the abdomen with the cone at 90° elevation.

C. Mechanism Optimization

1) Workspace Requirements for a Minimally Invasive Surgical Robot With Practical Joint Limits: Analysis of an extensive database [24], [26] including the kinematics and dynamics of two MIS tools acquired during tissue handling/examination, tissue dissection, and suturing performed on animal models *in-vivo* by 30 surgeons indicated that 95% of the time the surgical tools were contained by a cone with a vertex angle of 60° with its tip located at the MIS port. A measurement taken on a human subject showed that in order to reach the full extent of the abdomen the endoscopic tool needed to move 90° in the lateral/medial direction (left to right) and 60° in the superior/inferior (foot to head) direction (Fig. 4).

The reachable workspace of the spherical manipulator is a sector of a sphere. The mechanism link angles (α_{ij}) and the range of motion of the joint angles $(\theta_i,)$ determine the size and shape of this sector. Based on the measurements performed *in-vivo*, we define a target workspace, t_{DWS}, the dexterous workspace (DWS) for the surgical robot, as the area on the sphere bounded by the intersection of the sphere with a right circular cone with vertex angle 60° located at the center. It is the workspace in which surgeons spend 95% of their time during tissue manipulation tasks. Similarly, we define, t_{EDWS}, the extended dexterous workspace (EDWS) with vertex angle 90° to accommodate the workspace required to reach the full extent of the human abdomen without reorientation of the manipulator relative to the patient.

Kinematic analysis does not consider mechanism design constraints, in particular, joint limits. Based on preliminary mechanical design of the serial manipulator, the range of motion for the first joint angle is 180° $(0° < \theta_1 < 180°)$ and the range of motion for the second joint is 160° $(20° < \theta_3 < 180°)$. By adding these joint limits into the optimization, the true reachable workspace of a physically implemented device can be analyzed.

2) Mechanism Isotropy: The Jacobian matrix allows one to analyze the kinematic performance of a mechanism. Several performance metrics have been proposed including the manipulability measure [29] and mechanism isotropy [30]. Isotropy defined as the condition number of the Jacobian and like manipulability ranges from 1 to infinity. It is a measure of directional uniformity, i.e., how well the mechanism can move in all directions. An early design choice was to use the same actuators for both degrees of freedom. Assuming that the surgical motion demands are uniform with respect to the robot in the surgical site, a

good isotropy score would indicate that the load on the motors of the two joints would be similar. We would like to use a bounded scoring criterion so we redefine isotropy for our use as the reciprocal of the condition number of the Jacobian matrix. This allows the score to range from 0 to 1, 0 being a singularity and 1 being perfectly isotropic. It will be further shown that the isotropy for this manipulator is only dependent on the elbow joint angle (θ_3).

$$ISO(\theta_1, \theta_3) = \frac{\sigma_{min}}{\sigma_{max}} \quad ISO \in \langle 0, 1 \rangle. \tag{8}$$

3) Dynamic Penalty: If mechanism isotropy were the only performance criteria used, the solution to the design space search would result in 90° links. This is because kinematic measures tend to favor longer links, allowing the elbow joint angle to deviate as little as possible from the isotropic pose while still reaching the target workspace. However, longer links reduce stiffness and increase mass and inertia. The aim is to produce the smallest, best performing mechanism possible for the surgical manipulator. Thus, the scoring criterion should also contain a dynamic term that penalizes longer links. Based on long beam theory, the mechanism's stiffness is inversely proportional to the cube of the total link length [31].

4) Scoring Criteria and Cost Function: The sets D, P, and T are defined for the optimization.
- D: the set of all designs, d, which are pairs of link angles, $(\alpha_{13}, \alpha_{35})$.
- P: the set of all points, p, in the reachable workspace of the design d.
- T: the set of all possible target workspaces, t, within P. Each target workspace has a constant area, a_t. Specifically, t is either t_{DWS} or t_{EDWS}.

The following scores are defined:
- Each pair $\{d, p\}$ has a score s_{dp}, associated with the design and the pose of the manipulator

$$s_{dp} = \frac{ISO(\theta_3)}{(\alpha_{13} + \alpha_{35})^3}.$$

- The target t is composed of points p and has a score ζ_t

$$\zeta_t = \frac{1}{a_t} \sum_t (s_{dp}) \min_t (s_{dp}).$$

- Each design d has a score γ_d

$$\gamma_d = \max_T (\zeta_t).$$

The optimal design d_{opt} is the design associated with the score ζ_{opt}

$$\zeta_{opt} = \max_D (\gamma_d).$$

Combining, the optimal candidate score

$$\zeta_{opt} = \max_D \left(\max_T \left(\frac{1}{a_t} \sum_t (s_{dp}) \min_t (s_{dp}) \right) \right).$$

The composite target score ζ_t is composed of three components. The summation of point scores over the target workspace gives an indication of overall performance within the workspace. Multiplication by the minimum point score penalizes the target score if the workspace is
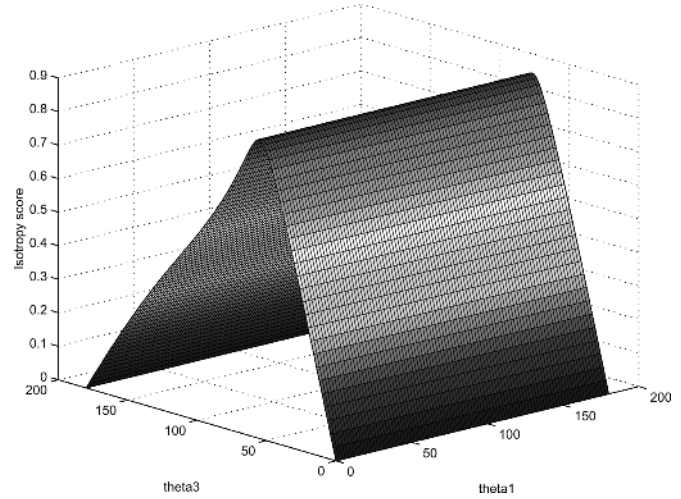

Fig. 5. Isotropy score as a function of θ_1 and θ_3 for the design ($\alpha_{13} = 60°$, $\alpha_{35} = 50°$). Observe that for a fixed design, isotropy is purely a function of θ_3, the elbow joint angle.

near a singularity. Dividing by the area, a_t, normalizes the score with respect to larger or smaller workspaces (DWS versus EDWS).

5) Optimization Algorithm: The optimization algorithm follows several steps. First, the appropriate design space D is defined. For each candidate d and manipulator pose p in P, the score, s_{dp}, is calculated via the inverse kinematics. In each set of target workspaces T, the target workspace t is moved around the reachable workspace P and for each t in T, ζ_t is calculated. Then a score γ_d is assigned for the design d. Over the design space D the best performing candidate d is found and associated with the score ζ_{opt}.

The optimization was run for both the DWS and EDWS with and without the joint limits. The results from the EDWS show which designs can fully reach t_{EDWS} (those designs with a nonzero score). This information was used as a 'filter' on the DWS dataset to determine the best performing mechanism over the DWS that contained the EDWS in its workspace. This optimization algorithm leads to a highly dexterous mechanism within a specific workspace that can also reach the entire workspace required for surgery.

III. RESULTS

A. Experimental Evaluation

Different combinations of serial and parallel mechanisms with varying link angles were tested on an anthropomorphic human plastic torso. In both serial and parallel configurations, mechanisms with 90° links suffered robot-patient collisions. Using two parallel mechanisms, even the most compact configuration (60° links) created self-collisions. A minimum distance between the two mechanisms of 30 cm was required in order to avoid robot-robot collision. Similar constraints were observed for a hybrid configuration with a combination of one serial and one parallel mechanism. The fewest collision problems were encountered with both mechanisms in serial configurations [Fig. 2(c)].

Based on preliminary kinematic optimization results, two serial arms were used in a minimally invasive surgical set up using a pig as an animal model. The two arms, each configured with 75° links, provided sufficient range of motion while avoiding collisions during gross and dexterous manipulations.

B. Kinematic Optimization

The recursive formulation of the Jacobian matrix contains the rotation matrices $[^5R_1]$ and $[^5R_3]$ which are functions of θ_3 and θ_5 re-
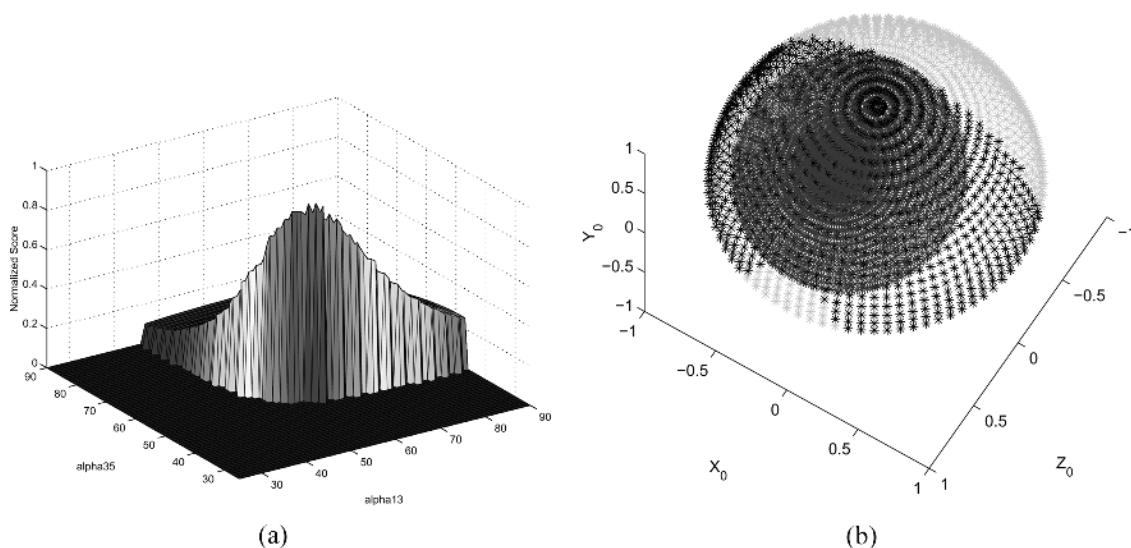
Fig. 6. (a) The normalized score of the serial mechanism as a function of the link length angles Link1 (α_{13}) and Link2 (α_{35}) along with (b) the workspace of the mechanism with the best performance link angles $\alpha_{13} = 60°$, $\alpha_{35} = 50°$.

TABLE II
OPTIMAL DESIGNS FOR THE DIFFERENT TARGET WORKSPACES, WITH AND
WITHOUT JOINT LIMITS, RESULTS EXPRESSED AS (α_{13}, α_{35}) IN DEGREES

Data Set	Without Joint Limits	Without Joint Limits
DWS Optimal	(33°,32°)	(42°,38°)
EDWS Optimal	(54°,51°)	(64°,55°)
DWS Optimal constrained to reach EDWS	(46°,44°)	(60°,50°)

spectively. Because $\theta_5 = 0$ and is not considered in this analysis, the Jacobian is a function of only θ_3, the elbow angle. Fig. 5 shows the mechanism isotropy of the ($\alpha_{13} = 60°$, $\alpha_{35} = 50°$) design as a function of elbow joint angle (θ_3) and shoulder joint angle (θ_1).

Table II summarizes the "optimal" designs with and without the joint limit constraints. The "DWS Optimal" set is a kinematic optimization run with the target workspace as t_{DWS}, the workspace in which surgeons spend 95% of their time. The "EDWS Optimal" set is a kinematic optimization run with the target workspace as t_{EDWS}, the workspace required to reach the entire abdominal cavity. The 'DWS Optimal constrained to EDWS' set is the kinematic optimization run with the target workspace as t_{DWS}, but only the designs that could reach the EDWS were included. The "DWS Optimal constrained to EDWS" with joint limits is the set most applicable to the actual surgical robot design and is the most compact design that can reach the entire abdominal cavity while having higher performance within the region that surgeons occupy the majority of their time. Fig. 6(a) shows the candidate scores, γ_d, over the design space D. Fig. 6(b) outlines the reachable workspace of the optimal design ($\alpha_{13} = 60°$, $\alpha_{35} = 50°$) with the EDWS superimposed over it.

C. Surgical Robot Prototype

Fig. 7 shows the ultimate result from this work, a surgical robot following a macro-micro approach. The robot is a 6-DOF cable actuated system with all the actuators located on a static base. The first two DOF, optimized as part of this study, are the shoulder and elbow joints that position the MIS tool in space. The tools are modified from Computer Motion Zeus Endo-Wrist tools. The robot supports tool positioning, tool roll, one or two wrist axes, and grasping.
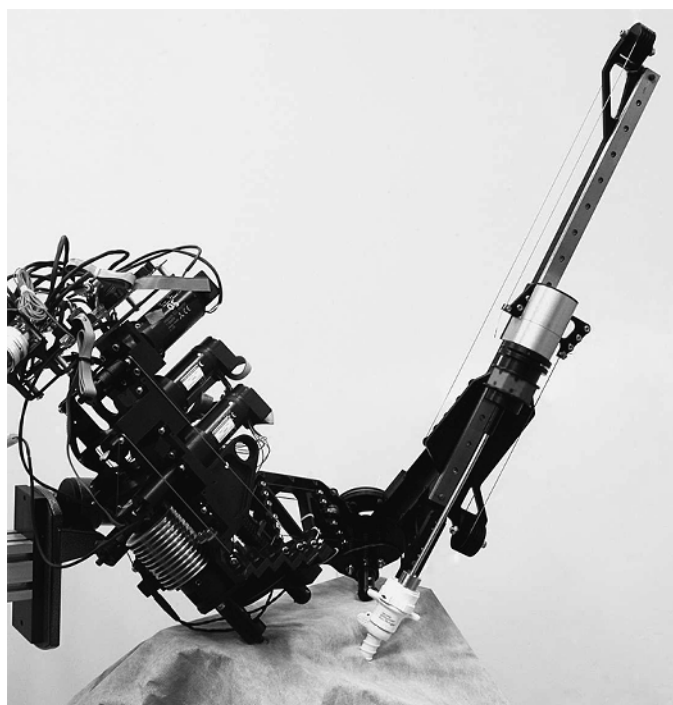

Fig. 7. The University of Washington BioRobotics Lab prototype surgical robot has link angles optimized specifically for the clinical requirement of MIS. It is cable-driven with all actuators located on a static base.

IV. DISCUSSION

This study focuses on the design methodology for a new lightweight and compact surgical manipulator for MIS. Due to the pivot constraint of MIS it is only natural to evaluate a spherical mechanism as a design candidate for a surgical robot. Both serial and parallel configurations were considered, each with their own strengths and weaknesses. The surgeons' experiments with the passive mockup were an initial yet critical qualitative investigation into the practicality of the spherical mechanism. Identification and understanding of the three types of collisions faced in the surgical setting (self-collision, robot-robot and robot-patient collision) allows unsuitable designs to be eliminated prior to the

mathematical analysis. By using some very preliminary optimization data, the surgeons were able to not only test for range of motion, but also perform *in-vivo* surgical tasks on a porcine model. Among the various arm configurations of serial and parallel spherical mechanisms that were tested, the experimental results indicate that serial mechanism is the best configuration.

Following the experimental evaluation, the optimization algorithm aimed to define the smallest mechanism configuration that would satisfy the workspace requirements associated with MIS. The resultant design takes into account joint limits and the need to reach the entire EDWS while performing optimally within the DWS. As such, these results provide a design specification for a spherical manipulator for a MIS surgical robot.

The surgical robot developed from this work will be subject to rigorous clinical studies. The complete system consists of two 6 or 7-DOF manipulators positioned by a multiple degree of freedom positioning arm, following a macro-micro approach similar to the human arm and hand. It is comprised of two separate manipulators: a gross positioning mechanism corresponding to the human arm and a high dexterity surgical robot serving as the human hand.

While the results yield a compact, high performance manipulator, dynamic performance was not explicitly considered except the penalty proportional stiffness (link length cubed penalty). The performance criteria, s_{dp}, is at the core of the optimization. A future study will evaluate different performance criteria, both kinematic and dynamic in nature. A complete optimization of the surgical scene may include the placement of two or more manipulators and an endoscope positioned over a patient. It could consider practical design constraints such as robot-patient collisions as well as robot-robot collisions and self-collision. A complete analysis of the entire surgical scene (patient, multiple manipulators, camera positioner, etc.) along with kinematic and dynamic optimization of the manipulators could yield a result that truly defines an optimal solution for a set of surgical robotic applications.

ACKNOWLEDGMENT

REFERENCES

[1] S. Venema, "Experiments in surface perception using a haptic display," Ph.D. thesis, University of Washington, Seattle, Apr. 1999.

[2] J. Rosen, B. Hannaford, M. MacFarlane, and M. Sinanan, "Force controlled and teleoperated endoscopic grasper for minimally invasive surgery—experimental performance evaluation," *IEEE Trans. Biomed. Eng.*, vol. 46, no. 10, pp. 1212–1221, Oct. 1999.

[3] S. Sastry, M. Cohn, and F. Tendick, "Milli-robotics for remove, minimally invasive surgery," *J. Robot. Auton. Syst.*, vol. 21, no. 3, Sept. 1997.

[4] R. Taylor, S. Lavallee, G. Burdea, and R. Mosges, *Computer-Integrated Surgery*. Cambridge, MA: MIT Press, 1996.

[5] R. Howe and Y. Matsuoka, "Robotics for surgery," in *Annu. Rev. Biomed. Eng.*, 1999, vol. 1, pp. 211–240.

[6] G. Buess, M. Schurr, Fisher, and C. Sabine, "Robotics and allied technologies in endoscopic surgery," *Arch. Surg.*, vol. 135, pp. 229–235, 2000.

[7] K. Cleary and C. Nguyen, "State of the art. in surgical robotics: clinical applications and technology challenges," *Comput. Aided Surg.*, vol. 6, pp. 312–328, 2001.

[8] F. Ballantyne, *Surg. Laparosc., Endosc. Percutaneous Tech. (Special Issue Surg. Robot.)*, vol. 12, 2002.

[9] J. Speich and J. Rosen, "Medical robotics," in *Encyclopedia of Biomaterials and Biomedical Engineering*. New York: Marcel Dekker.

[10] A. Farz and S. Payandeh, "A robotic case study: optimal design for laparoscopic positioning stands," *Int. J. Robot. Res.*, vol. 17, no. 9, Sep. 1998.

[11] T. Li and S. Payandeh, "Design of spherical parallel mechanisms for application to laparoscopic surgery," *Robotica*, vol. 20, 2002.

[12] J. Shi, P. Mederic, V. Pasui, G. Morel, and S. Wang, "Preliminary results on the design of a novel laparoscopic manipulator," presented at the Proc. 11th World Congr. Mechanism and Machine Science, China, Apr. 2004.

[13] R. Satava, "Disruptive visions: the operating room of the future," *Surgical Endosc.*, vol. 17, no. 1, 2003.

[14] Intuitive Surgical [Online]. Available: http://www.intuitivesurgical.com

[15] G. Guthart and K. Salisbury, "The inituitive telesurgical system: overview and application," in *Proc. 2000 IEEE ICRA*, 2000, pp. 618–621.

[16] A. J. Madhani, G. Niemeyer, J. Salisbury, and J. K. , "The black falcon: a teleoperated surgical instrument for minimally invasive surgery," in *Proc. IEEE/RSJ Int. Conf. Intelligent Robots and Systems*, 1998, pp. 936–944.

[17] Computer Motion [Online]. Available: http://www.computermotion.com

[18] J. Marescaux, J. Leroya, M. Gagner, F. Rubino, D. Mutter, M. Vix, S. Butner, and M. Smith, "Transatlantic robot-assisted-telesurgery," *Nature Mag.*, vol. 413, 2001.

[19] R. Taylor, H. Paul, B. Mittelstad, E. Glassman, B. Mustis, and W. Bargar, "Robotic total hip replacement surgery in dogs," in *Proc. Int. Conf. IEEE Engineering in Medicine and Biology Soc., (IEEEEMBS)*, 1989, vol. 11, pp. 887–888.

[20] R. Kurtz and V. Hayward, "Multiple-goal kinematic optimization of a parallel spherical mechanism with actuator redundancy," *IEEE Trans. Robot. Autom.*, vol. 8, no. 5, pp. 644–651, Oct. 1992.

[21] J. Merlet, *Parallel Robots*. Norwell, MA: Kluwer Academic, 2000.

[22] M. Ouerfelli and V. Kumar, "Optimization of spherical five-bar parallel drive linkage," *ASME J. Mech. Design*, vol. 116, pp. 166–173, Mar. 1994.

[23] M. Lum, J. Rosen, M. Sinanan, and B. Hannaford, "Kinematic optimization of a spherical mechanism for a minimally invasive surgical robot," in *Proc. 2004 IEEE Conf. Robotics and Automation*, New Orleans, LA, Apr. 2004, pp. 829–834.

[24] J. Rosen, J. Brown, L. Chang, M. Barreca, M. Sinanan, and B. Hannaford, "The bluedragon—a system for measuring the kinematics and the dynamics of minimally invasive surgical tools in vivo," in *Proc. IEEE Intl. Conf. Robotics and Automation ICRA-2002*, Arlington, VA, May 2002, pp. 1876–1881.

[25] J. Brown, "*In-vivo* and postmortem biomechanics of abdominal organs under compressive loads: experimental approach in a laparoscopic surgery setup," Ph.D. thesis, University of Washington, Seattle, Dec. 2003.

[26] J. Rosen, J. Brown, L. Chang, M. Sinanan, and B. Hannaford, "Generalized approach for modeling minimally invasive surgery as a stochastic process using a discrete markov model," *IEEE Trans. Biomed. Eng.*, vol. 53, no. 3, pp. 399–413, Mar. 2006.

[27] M. Lum, "Kinematic optimization of a 2-DOF spherical mechanism for a minimally invasive surgical robot," MSEE thesis, , , Dec. 2004.

[28] J. J. Craig, *Introduction to Robotics*, 2nd ed. Reading, MA: Addision Wesley, 1989.

[29] T. Yoshikawa, "Manipulability of and redundancy control robotic mechanisms," *Int. J. Robot. Res.*, vol. 4, no. 2, pp. 1004–1009, 1985.

[30] J. Salisbury and J. Craig, "Articulated hands: force control and kinematic issues," *Int. J. Robot. Res.*, vol. 1, no. 1, pp. 4–17, 1982.

[31] Gere and Timoshenlo, *Mechanics of Materials*, 4th ed. Boston, MA: PWS, 1990.